

Analytic Design Method for (Integrated-) Transformers of Resonant Converters using Extended Fundamental Frequency Analysis

Jürgen Biela *
Johann W. Kolar **

Abstract – The series-parallel resonant converter and its magnetic components are analysed by fundamental frequency techniques. The proposed method allows an easy design of the integrated transformer and the calculation of the losses of all components of the converter. Thus, an optimisation of the whole converter system – minimising either the volume and/or the losses of the converter (upper temperature is restricted) – could be done based on the derived set of equations. Moreover, the equations also include a ZCS condition for one leg of the converter, the control of the converter by the frequency *and* duty cycle and a load with offset voltage.

The proposed analytic model is validated by simulation as well as by experimental results.

Keywords: fundamental frequency analysis, transformer design, reluctance model, resonant converter, integrated transformer, optimisation

List of Symbols

V_{IN}	DC input voltage
V_{AB}	Converter output voltage
$V_{AB(1)}$	Fundamental component of V_{AB}
V_{OUT}	Output voltage
V_{CP}	Voltage across C_P
$V_{CP(1)}$	Fundamental component of V_{CP}
V_{Off}	Offset voltage of load (cf. Fig. 1)
C_S	Series capacitor
L_S	Resonant inductor
C_P	Parallel capacitor
I_P	Primary current
I_S	Secondary current
I_R	Rectifier input current
$I_{R(1)}$	Fundamental component of I_R
I_{OUT}	Output current
ω	Angular switching frequency
Z	Fundamental frequency impedance of the resonant circuit with load

Z_{CpR}	Fundamental frequency impedance of C_P in parallel with the rectifier
α	Angle between resonant current I_S zero-crossing and start of rectifier commutation
β	Angular duration of zero voltage state in discontinuous parallel capacitor voltage waveform
D	Duty cycle
N_P	Number of primary turns
N_S	Number of secondary turns
R	Load resistance
R_V	Internal resistance of voltage source $V_{AB(1)}$ (cf. Fig. 4)
\mathcal{R}_{M1}	Magnetic reluctance of the transformer leg carrying the primary winding
\mathcal{R}_{M2}	Magnetic reluctance of the transformer leg carrying the secondary winding
\mathcal{R}_σ	Magnetic reluctance of the leakage path (including air gap)

1. Introduction

Applying resonant DC-DC converters can help to reduce the switching losses and / or to raise the switching frequency of the power switches. On this account the overall system size in many industrial applications, e.g., telecom power supplies [1], high voltage generators [2] or inductive heating [3] could be reduced. Especially, the series-parallel resonant converter, **Fig. 1**, is a promising converter structure since it combines the advantages of the series resonant converter and the parallel resonant converter. On the one hand the resonant current decreases with the decrease of the load and the converter can be regulated at no load and on the other hand good part-load efficiency can be achieved [4 & 5]. Furthermore, the converter is naturally short circuit proof.

The resonant circuit (C_S , L_S and C_P) of the series-parallel resonant converter is fed by a square wave input voltage V_{AB} which usually has a varying frequency and duty cycle. In order to achieve a ZVS condition in one leg of the converter and to prevent a MOSFET from a hard turn-off of a diode the operating frequency of the converter has to be

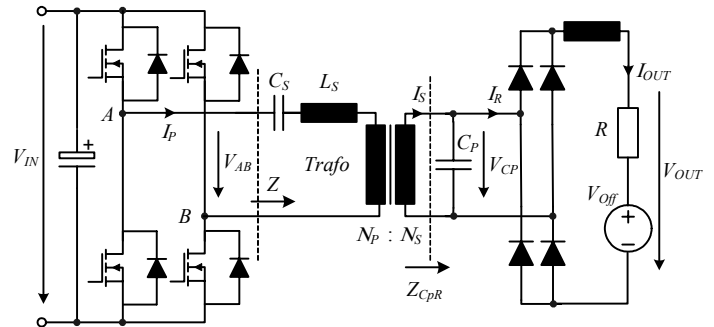


Fig. 1. Series-parallel resonant DC-DC converter always above the resonant frequency of the resonant circuit which is dependent on the load of the converter [2]. The square wave input voltage is filtered by the resonant circuit so that the current in the resonant components is almost sinusoidal (**Fig. 2**). Neglecting the small harmonics of the resonant current the analytic calculation of the resonant converter can be done by simple AC circuit analysis where the square wave input voltage V_{AB} , the square wave rectifier input current I_R and the not sinusoidal voltage across the parallel capacitor V_{CP} are represented by their respective fundamental components. This method was proposed in [5].

Under heavy load conditions, however, the voltage waveform of the parallel capacitor V_{CP} is clamped by the output current to zero for a certain period of time, period β

* Power Electronic Systems Laboratory, ETH Zürich, biela@lem.ee.ethz.ch Physikstrasse 3, CH-8092 Zürich, Switzerland

** Power Electronic Systems Laboratory, ETH Zürich, kolar@lem.ee.ethz.ch Physikstrasse 3, CH-8092 Zürich, Switzerland
Homepage: www.pes.ee.ethz.ch

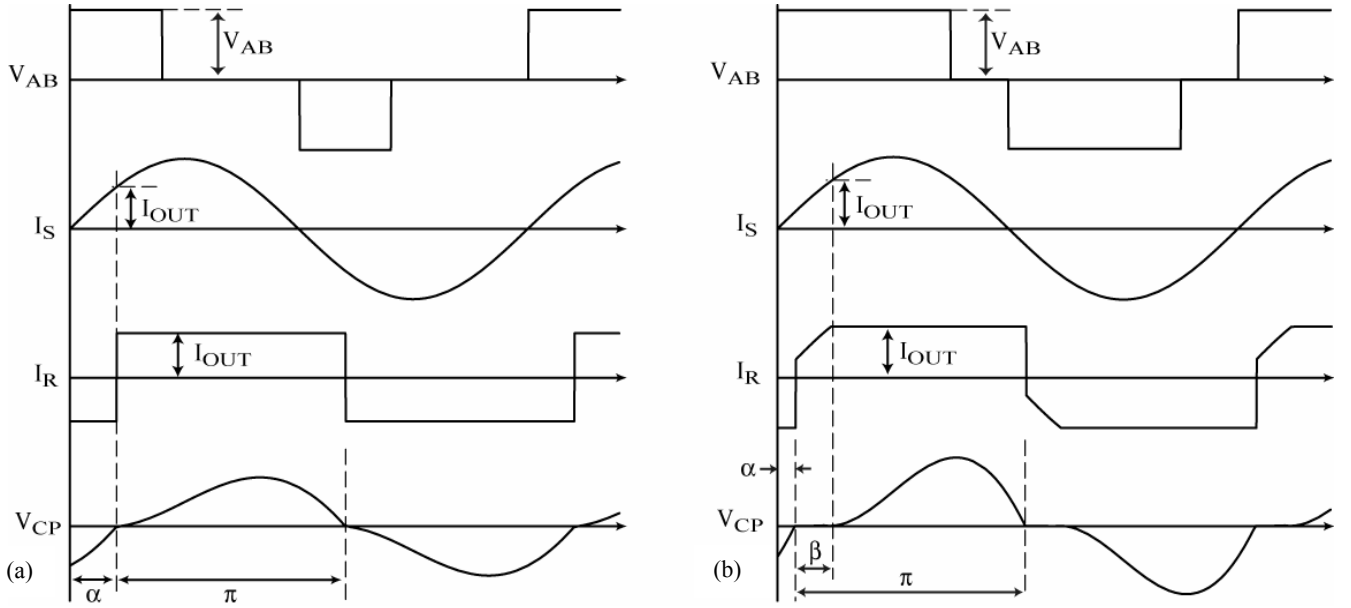


Fig. 2. (a) Converter output voltage V_{AB} , primary current I_p , rectifier current I_R and parallel capacitor voltage V_{CP} in continuous capacitor voltage mode. (b) The same waveforms as for (a) but for discontinuous capacitor voltage mode (assumption: magnetizing current $I_\mu = 0$)

in Fig. 2(b), which leads to a distorted and discontinuous parallel capacitor voltage V_{CP} . Under these conditions the standard fundamental frequency analysis is inaccurate. Therefore, the authors of [6] proposed an extended fundamental frequency analysis which accounts for the discontinuous capacitor voltage under heavy load conditions. This method uses two different models of the resonant converter – one for the continuous operation mode and one for the discontinuous mode and yields quite accurate results for all operating conditions (light, part, and heavy load). The equations of this model are based on the assumption of a negligible ripple of the output current.

With this analytic model the design of the resonant circuit including the voltage transfer ratio of the transformer could be performed quite accurately. The design of the transformer itself, however, is still elaborate since the current respectively voltage waveforms and their phase relation for the primary and secondary windings are required in order to be able to calculate the flux distribution within the core. This is particularly true if the series inductance is realised by the leakage inductance of the transformer which is increased by a magnetic shunt [7 -10]. Depending on the winding geometry/core structure the three flux parts – primary linked flux, secondary linked flux and leakage flux – add or subtract in the different legs of the transformer whereby the absolute values and the phase relations of the fluxes have to be considered. Especially in the magnetic shunt the phase relations between the different flux parts must be considered in order to design the magnetic device properly.

For this reason the analytic model proposed in [6] is extended in this paper by a magnetic reluctance model of the transformer which includes the series inductance which is realised by the leakage inductance of the transformer. In Fig. 4 the series-parallel resonant converter with the reluctance model is shown. The presented reluctance model represents a simple E-core transformer where the windings are placed on the two outer legs of the core and the mag-

netic shunt / leakage path is implemented by the centre leg (Fig. 3) but basically every core geometry and winding structure could be modelled in this way. The series inductance is controlled by the air gap in the centre leg. The derivation of the reluctance model is shortly presented in **section 2** before the analytic equations for the series-parallel resonant circuit including the reluctance model are presented in **section 3**.

Furthermore, the equations of [6] are extended for an operation mode where one leg of the converter is switched at the zero crossing of the resonant current I_p (Fig. 5). This is a known method to reduce the switching losses (ZCS) of the converter. The control of the output voltage/current by the duty cycle *and* the switching frequency is also described by the extended set of equations which are presented in section 3.

After the derivation of the model the analytic results are validated by circuit simulations using SIMPLORERTM and measurements on different prototypes. The results of the comparison and the discussion are presented in **section 4**. Finally, a conclusion and topics of future research are given in **section 5**.

2. Magnetic Circuit Model

In the following a short summary of magnetic circuit models based on [11] and the derivation of the equations which are applied in the calculations in section 3 is given.

By means of magnetic circuit models Ampere's law is simplified so that the line and surface integral do not have to be evaluated in order to find the flux distribution within the magnetic core. This simplification is based on the following two assumptions. Firstly, the absolute value of the magnetic field \vec{H} is constant in a given volume and secondly, the direction of the magnetic field \vec{H} is aligned with the direction of the path of integration.

With this assumptions Ampere's law simplifies to

$$\oint_l \vec{H} \cdot d\vec{l} = \iint_S \vec{J} \cdot d\vec{s} \Rightarrow H \cdot l = N \cdot I. \quad (1)$$

Applying the relationship between the flux density B and the magnetic field and the definition of the flux yields

$$\left. \begin{aligned} \vec{B} &= \mu_0 \cdot \mu_r \cdot \vec{H} \\ \Phi &= B \cdot A_e \end{aligned} \right\} \Phi \cdot \frac{l}{\mu \cdot A_e} = \Phi \cdot \mathfrak{R} = N \cdot I. \quad (2)$$

The quantity \mathfrak{R} is referred to as the magnetic reluctance (of the path l) and the product $N \cdot I$ is known as the magneto motive force (mmf). Equation (2) represents Ohm's law for magnetic circuits which is the magnetic analogue to the Ohm's law for electric circuits: $R \cdot I = U$, i.e. the flux corresponds to the current and the mmf to the voltage. With this equation and above mentioned assumptions also Kirchhoff's voltage law (VL) and current law (CL) can be applied to the magnetic circuit.

$$\begin{aligned} VL: N \cdot I &= \Phi \cdot (\mathfrak{R}_1 + \mathfrak{R}_2 + \dots + \mathfrak{R}_n) \quad (\text{for a given path}) \\ CL: \Phi_1 + \Phi_2 + \dots + \Phi_n &= 0 \quad (\text{for a given node}) \end{aligned} \quad (3)$$

Thus, by solving the system equation of the magnetic circuit the flux distribution in the core can be calculated. The application of Faraday's law then leads to the induced voltage

$$V = \frac{d\Psi}{dt} = N \cdot \frac{d\Phi}{dt}. \quad (4)$$

Assuming that the flux varies sinusoidally with time (4) can be rewritten as

$$\underline{V} = j \cdot \omega \cdot \underline{\Phi}. \quad (5)$$

In (5) \underline{V} is the complex voltage vector and $\underline{\Phi}$ is the complex vector of the magnetic flux.

The above mentioned assumptions for applying magnetic circuit theory are approximately fulfilled in regions of high permeability (e.g. ferrite core) if, among other things, the skin effect of magnetic fields is neglected for HF-applications. Usually, in air gaps the magnitude of the magnetic field is not constant over the cross section because of fringing flux. For calculating the magnetic reluctance of air gaps empirical and FEM-based models [12, 13 & 14] have been proposed. Here the flux density / exact magnetic field distribution is not important (no losses are generated in the gap) but only the overall magnetic reluctance seen by the flux is needed for the calculations.

In principle, it is possible to model the magnetic device very accurately with magnetic reluctances (with an increasing number of modelled magnetic paths) but usually a quite simple model is enough for getting reasonably exact results. In **Fig. 3(a)** an E-core with two windings on its outer legs and the definition of the directions for the quantities is given. With this winding structure the centre leg carries the leakage flux ($\Phi_P - \Phi_S$) and the leakage inductance is adjusted to the needed value by the air gap in this leg. Below, in **Fig. 3(b)**, the appropriate magnetic circuit model is given for sinusoidal fluxes.

Applying the magnetic analogue of Kirchhoff's voltage law, (3), to the two loops of the magnetic circuit in **Fig. 3(b)** yields the following two equations

$$\begin{aligned} N_P I_P &= \mathfrak{R}_{M1} \Phi_P + \mathfrak{R}_\sigma \cdot (\Phi_P - \Phi_S) \\ N_S I_S &= -(\mathfrak{R}_{M2} \Phi_S + \mathfrak{R}_\sigma \cdot (\Phi_S - \Phi_P)) \end{aligned} \quad (6)$$

Solving these equations for the flux values and using $U = N \cdot d\Phi/dt = L \cdot dI/dt$ leads to the following relations between the magnetic reluctances and the inductances.

$$\begin{aligned} L_1 &= \frac{N_P^2 \cdot (\mathfrak{R}_{M2} + \mathfrak{R}_\sigma)}{\mathfrak{R}_{M1} \mathfrak{R}_{M2} + \mathfrak{R}_{M1} \mathfrak{R}_\sigma + \mathfrak{R}_\sigma \mathfrak{R}_{M2}} \\ L_2 &= \frac{N_S^2 \cdot (\mathfrak{R}_{M1} + \mathfrak{R}_\sigma)}{\mathfrak{R}_{M1} \mathfrak{R}_{M2} + \mathfrak{R}_{M1} \mathfrak{R}_\sigma + \mathfrak{R}_\sigma \mathfrak{R}_{M2}} \\ L_{\sigma(P)} &= \frac{N_P^2}{\mathfrak{R}_{M1} + \mathfrak{R}_\sigma} \quad L_{\sigma(S)} = \frac{N_S^2}{\mathfrak{R}_{M2} + \mathfrak{R}_\sigma} \end{aligned} \quad (7)$$

The inductance L_1 can be measured at the primary side when the secondary is left open and L_2 is the same for the secondary side. Additionally, the equation for the complete leakage inductance is given - one referred to the primary side $L_{\sigma(P)}$ and one to the secondary side $L_{\sigma(S)}$. With the above equations the analytic model for the series-parallel resonant converter including the transformer could be set up in the following section.

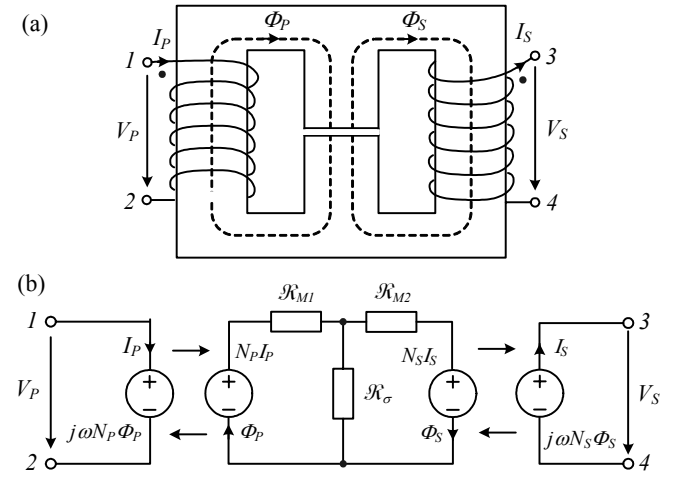


Fig. 3. (a) Transformer on E-core (the middle leg carries the leakage flux) (b) Magnetic circuit model of the transformer

3. Analysis of the Extended Model

As already mentioned the following considerations for the series-parallel resonant converter shown in **Fig. 4** are partly based on the fundamental frequency analysis proposed in [6]. The method of [6] has been extended by a reluctance model for the transformer with its leakage inductance, a ZCS condition for one leg and the control by frequency and duty cycle. As far as possible and reasonable the notation used in [6] has been retained.

The calculations are based on the assumptions that both the primary resonant current I_P and the secondary resonant current I_S are sinusoidal, that the output current is constant and that the components are ideal. The major procedure of the analysis is to determine the fundamental frequency impedance \underline{Z}_{CpR} of the parallel connection of C_P and the rectifier at first. With this impedance the input impedance \underline{Z} of the resonant circuit, seen by the converter / voltage source V_{AB} , could be calculated. In the impedance \underline{Z} also the reluctance model of the transformer is included. In the next step two equations can be set up. The first one describes the relation between the phase shift of the primary current I_P and $\underline{V}_{AB(t)}$ (**Fig. 5**), which is determined on the one hand by the duty cycle D and on the other hand by \underline{Z} . The second expression relates the output voltage V_{OUT} of the converter to the load voltage which is given by the load characteristic (V_{off} & R) and the output current I_{OUT} . These two equations

together with one (CCM) or two (DCM) additional equations describe the behaviour of the system. The duty cycle D and the output current / voltage now can be calculated numerically for a given frequency f and load characteristic (V_{off} & R) or vice versa.

3.1 Fundamental frequency impedance \underline{Z}_{CPR} In the following the impedance \underline{Z}_{CPR} is calculated for the DCM (Fig. 2(b)) by first considering the fundamental component of the rectifier input current $\underline{I}_{R(1)}$ (cf. Fig. 4) (~(1) in [6]).

$$\underline{I}_{R(1)} = \frac{2j}{\pi} \left[\int_{\alpha}^{\alpha+\beta} I_S \cdot \sin \theta \cdot e^{-j\theta} d\theta + \int_{\alpha+\beta}^{\alpha+\pi} I_{OUT} \cdot e^{-j\theta} d\theta \right]$$

$$\underline{I}_{R(1)} = \frac{2}{\pi} \left[\frac{I_S}{4} \cdot (2\beta - je^{-2j\alpha} \cdot (e^{-2j\beta} - 1)) + I_{OUT} \cdot (1 + e^{-j\beta}) e^{-j\alpha} \right] \quad (8)$$

Since the resonant current on the secondary \underline{I}_S is assumed to be sinusoidal the fundamental component of the capacitor voltage $\underline{V}_{CP(1)}$ could simply be calculated by AC circuit analysis and is given by (~(2) in [6])

$$\underline{V}_{CP(1)} = \frac{\underline{I}_S - \underline{I}_{R(1)}}{j\omega C_P} \quad (9)$$

Dividing the capacitor voltage $\underline{V}_{CP(1)}$ by the sinusoidal secondary resonant current \underline{I}_S yields the fundamental component of the secondary side impedance \underline{Z}_{CPR} (~(3) in [6])

$$\underline{Z}_{CPR} = \frac{\underline{V}_{CP(1)}}{\underline{I}_S} = \frac{2\pi - 2\beta + je^{-2j\alpha} \cdot (e^{-2j\beta} - 1) - 4 \frac{I_{OUT}}{I_S} (1 + e^{j\beta}) e^{j\alpha}}{2j\pi\omega C_P} \quad (10)$$

The impedance \underline{Z}_{CPR} for the CCM is obtained by setting $\beta = 0$ in (10).

3.2 Continuous Capacitor Voltage Mode (CCM) In the CCM the value of the resonant current I_S at the angle α (where V_{CP} falls to zero) is larger than I_{OUT} . The difference between the resonant current I_S and the output current I_{OUT} charges the capacitor C_P . Thus the time response of the capacitor voltage is given by (~(5) in [6])

$$V_{CP}(\theta) = \frac{1}{\omega C_P} \int_{\alpha}^{\theta} (I_S \cdot \sin \varphi - I_{OUT}) d\varphi$$

$$= \frac{I_S (\cos \alpha - \cos \theta) - I_{OUT} (\theta - \alpha)}{\omega C_P} \quad (11)$$

for $\alpha \leq \theta \leq \alpha + \pi$. Since the capacitor voltage is periodic for steady state operation it must fall to zero at the end of each cycle. Evaluating (11) under this condition yields an expression for α (~(6) in [6]).

$$V_{CP}(\alpha + \pi) = 0 \Rightarrow \alpha = \arccos \left(\frac{I_{OUT} \cdot \pi}{2I_S} \right) \quad (12)$$

Furthermore, the average value of the capacitor voltage V_{CP} must be equal to the output voltage

V_{OUT} because the volt-seconds across the output inductor must be balanced. Calculating the average value of V_{CP} according to (11) and using (12) for substituting I_{OUT} results in (~(7) in [6])

$$V_{OUT} = \frac{1}{\pi} \int_{\alpha}^{\alpha+\pi} V_{CP}(\varphi) d\varphi = \frac{2I_S \sin \alpha}{\pi \omega C_P} \quad (13)$$

Another equation for α may be obtained by inserting the output voltage $V_{OUT} = V_{off} + R \cdot I_{OUT}$ (equal to the load voltage) in (13) and solving for $\sin(\alpha)$. The resulting equation must be divided by (12) which has to be solved for $\cos(\alpha)$ first. This results in

$$\alpha = \arctan \left(\frac{\omega C_P \cdot (V_{off} + R \cdot I_{OUT})}{I_{OUT}} \right) \quad (14)$$

which is the first system equation for the CCM (~(8) in [6]). By setting $\beta = 0$ in (10) the impedance \underline{Z}_{CPR} for the CCM is obtained which may be simplified by substituting I_{OUT}/I_S using (12) (~(9) in [6])

$$\underline{Z}_{CPR} = \frac{1 - 8/\pi^2 \cdot e^{j\alpha} \cdot \cos \alpha}{j\omega C_P} \quad (15)$$

With (6), i.e. the description of the transformer (incl. L_S) and

$$\underline{I}_S = \frac{V_S}{\underline{Z}_{CPR}} = \frac{j\omega \cdot N_2 \cdot \Phi_S}{\underline{Z}_{CPR}} \quad (16)$$

the flux Φ_P and therewith the primary voltage $\underline{V}_P (= j\omega N_1 \Phi_P)$ of the transformer could be calculated as a function of \underline{I}_P and \underline{Z}_{CPR} . Applying Kirchhoff's voltage law to the most left mesh in Fig. 4 yields

$$\underline{V}_{AB(1)} = R_V \cdot \underline{I}_P + \frac{\underline{I}_P}{j\omega C_S} + j\omega \cdot N_1 \cdot \underline{\Phi}_P$$

$$\Rightarrow \underline{Z} = \frac{\underline{V}_{AB(1)}}{\underline{I}_P} \quad (17)$$

Dividing $\underline{V}_{AB(1)}$ by the primary current \underline{I}_P results in the fundamental frequency input impedance \underline{Z} of the resonant circuit. By means of the phase of the impedance \underline{Z} the second system equation for the CCM could be set up. The phase shift between the fundamental component of the input voltage $\underline{V}_{AB(1)}$ and the resonant current \underline{I}_P is on the one hand determined by the phase of \underline{Z} . On the other hand this phase shift is determined by the ZCS condition and the duty cycle D (cf. Fig. 5). Equating both conditions yields

$$\frac{\pi}{2} (1 - D) = \arctan \left(\frac{\text{Im}(\underline{Z})}{\text{Re}(\underline{Z})} \right) \quad (18)$$

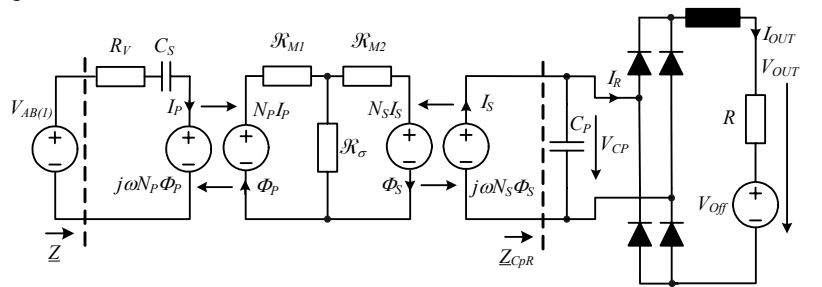


Fig. 4. Series-parallel resonant converter with reluctance model of the transformer. The converter output voltage V_{AB} is represented by its fundamental component $V_{AB(1)}$.

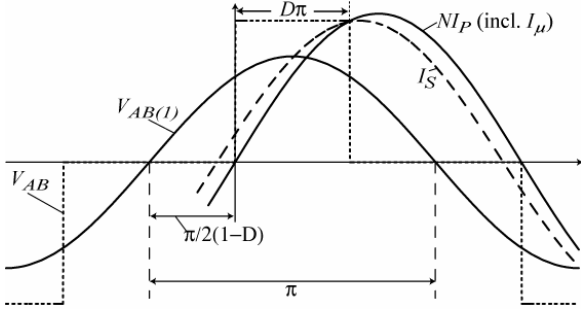


Fig. 5. Phase shift between $V_{AB(t)}$ and I_P (including magnetizing current I_μ) and between I_S and I_P (due to I_μ).

With the absolute value of the impedance Z the absolute value of the primary resonant current I_P could be calculated as

$$|I_P| = \frac{4}{\pi} V_{IN} \cdot \frac{\cos(\pi/2 \cdot (1-D))}{|Z|}. \quad (19)$$

Now the absolute value of I_S could be calculated with equations (6) by substituting I_P by (19) and $\underline{\phi}$ by means of (16). The resulting equation for $|I_S|$ is used for calculating the output voltage V_{OUT} by (13). This output voltage must be equal to the load voltage which is given by the load characteristic and the output current I_{OUT} .

$$V_{Off} + R \cdot I_{OUT} = \frac{2|I_S| \sin \alpha}{\pi \omega C_p} \quad (20)$$

Equation (20) is the third system equation for the CCM. By solving the three system equations [(14), (18) and (20)] numerically the output voltage V_{OUT} , the output current I_{OUT} , the duty cycle D and α can be calculated for a given frequency f and load characteristic V_{Off} & R or vice versa.

The CCM occurs if the resonant current I_S is larger than the output current I_{OUT} when the capacitor voltage V_{CP} falls to zero at the angle α . Therefore, the limit for the CCM is given by

$$I_S \sin \alpha > I_{OUT} \xrightarrow{\text{Eqn.13}} \frac{\omega C_p (V_{Off} + R I_{OUT})}{I_{OUT}} > \frac{2}{\pi}. \quad (21)$$

3.3 Discontinuous Capacitor Voltage Mode (DCM)

In contrast to the CCM the value of the resonant current I_S at the angle α (where V_{CP} falls to zero) is smaller than I_{OUT} in the DCM. As long as the resonant current I_S is smaller than I_{OUT} the capacitor voltage V_{CP} is clamped to zero by the negative difference between I_S and I_{OUT} [$-(I_S - I_{OUT})$] which flows through the rectifier diodes. From the angle β on I_S is larger than I_{OUT} and in the same manner as in CCM the positive difference between the currents ($I_S - I_{OUT}$) charges the capacitor C_p . Thus the capacitor voltage is given by (~(12) in [6])

$$\begin{aligned} \alpha &\leq \theta \leq \alpha + \beta \\ V_{CP}(\theta) &= 0 \\ \alpha + \beta &\leq \theta \leq \alpha + \pi : \\ V_{CP}(\theta) &= \frac{1}{\omega C_p} \int_{\alpha+\beta}^{\theta} (I_S \cdot \sin \varphi - I_{OUT}) d\varphi \\ V_{CP}(\theta) &= \frac{I_S (\cos(\alpha + \beta) - \cos \theta) - I_{OUT}(\theta - \alpha - \beta)}{\omega C_p}. \end{aligned} \quad (22)$$

Again, the average value of the capacitor voltage V_{CP} must

be equal to the output voltage. After carrying out the integration the expression could be simplified by using $I_S \cdot \sin(\alpha + \beta) = I_{OUT}$. The result of this operation is given in (~(14) in [6])

$$\begin{aligned} V_{OUT} &= \frac{1}{\pi} \int_{\alpha}^{\alpha+\pi} V_{CP}(\varphi) d\varphi \\ &= \frac{(\pi - \beta) \cdot I_S \cdot [\cos(\alpha + \beta) + \sin(\alpha)]}{\pi \omega C_p} + \\ &\quad + \frac{I_{OUT} \cdot (1 + \beta\pi - \beta^2/2 - \pi^2/2)}{\pi \omega C_p}. \end{aligned} \quad (23)$$

In the DCM two equations are needed for calculating the angles α and β . One is obtained by setting V_{CP} equal to zero at the end of every half cycle $V_{CP}(\alpha + \pi) = 0$ (~(15) in [6])

$$\cos(\alpha + \beta) + \cos(\alpha) + (\beta - \pi) \cdot \sin(\alpha + \beta) = 0. \quad (24)$$

The second one is given by $I_S \sin(\alpha + \beta) = I_{OUT}$ which relates the angles α and β with the absolute value of the resonant current on the secondary I_S and with the output current I_{OUT} . In order to eliminate I_S this equation is put in (23) which is set equal to the load voltage $V_{OUT} = V_{Off} + R \cdot I_{OUT}$. This results in (~(15) in [6]).

$$\begin{aligned} &(\pi - \beta) \cdot \cos(\alpha + \beta) + \sin(\alpha) + \sin(\alpha + \beta) \cdot \\ &\cdot \left[\left(1 + \beta\pi - \frac{\pi^2 + \beta^2}{2} \right) - \left(\frac{V_{Off}}{I_{OUT}} + R \right) \cdot (\omega\pi C_p) \right] = 0. \end{aligned} \quad (25)$$

The third and fourth system equation are given by (18) and (20) which are derived {by (16), (17) and (19)} in the same manner as described for the CCM except for setting $\beta = 0$ in Z_{CpR} in (16).

Due to the offset voltage of the load characteristic (25) is dependent on the output current I_{OUT} . Consequently, the two nonlinear equations for the angles α and β {(24) and (25)} must be solved numerically together with (18) and (20).

Instead of applying the described reluctance model for the magnetic device for calculating the flux distribution in the core it is also possible to use the standard network model equations of a transformer

$$\begin{aligned} V_P &= j\omega L_1 I_P + j\omega M I_S \\ V_S &= j\omega M I_P + j\omega L_2 I_S \end{aligned} \quad (26)$$

and calculate the flux through the primary and the secondary winding by

$$\underline{\phi}_P = \frac{I}{j\omega N_P} \cdot \underline{U}_P \quad \text{and} \quad \underline{\phi}_S = \frac{I}{j\omega N_S} \cdot \underline{U}_S. \quad (27)$$

For simple transformer designs the leakage flux could be approximated by the difference of the primary and the secondary flux. This is, however, limited to standard transformer designs. More sophisticated transformers (e.g. integrated magnetic devices or transformers with two magnetic shunts and/or leakage flux in the window) can not be described by the network equations as accurately as with the description of the device by magnetic reluctances. Furthermore, the magnetic reluctances directly depend on the geometry of the device what could be used in an optimisation

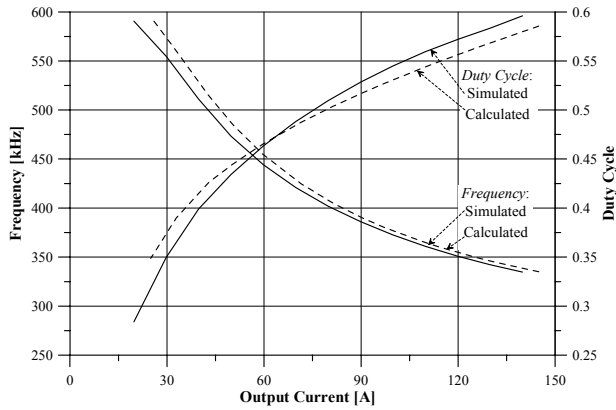


Fig. 6. Duty cycle D / frequency f against output current.
Solid lines: results of simulations.
Broken lines: predictions of proposed analytic model.

process of the converter. The values for L_1 , L_2 and M in (26) must either be measured or calculated by a FEA and/or a reluctance model. Thus, the approach with reluctance models is directly based on the physics and the geometry of the device and therefore is used for the proposed calculation method.

4. Validation of the Analytic Model

For validating the equations the results of the calculations are compared with simulation and measurement results in the following. First, the simulation results of a series-parallel resonant converter, which is operating in the CCM and the DCM, are compared with the analytic calculations. Thereafter, measurement and analytic results for a magnetically integrated transformer, which realises the series inductance of the resonant tank by its leakage inductance, are shown. Finally, measurement results for an electromagnetically integrated transformer are compared with the analytic calculations.

In **Fig. 6** the results for the operating frequency and the duty cycle of the analytic calculations and of the simulation of the series-parallel resonant converter are shown. The simulation is realised with SIMPLORER™ and includes a physical transformer model, where the flux values in the different legs of the transformer also can be simulated. The value of the resonant tank elements are:

- Series inductance $L_s = 12.5\mu\text{H}$
- Series capacitance $C_s = 35\text{nF}$
- Parallel capacitance $C_p = 110\text{nF}$

For these values the converter is in the CCM mode for light load (app. up to 45A output current) and in the DCM mode for heavy load. The crossover between the two analytic models describing the different modes is very smooth.

In **Fig. 7** the values for the flux through the primary and the secondary winding and the leakage flux are shown. As one can see the analytical results are in very good correspondence with the results of the simulation.

In the next step the analytic and the simulation results are compared with measurement results, which are obtained with the converter shown in **Fig. 8**. There, the resonant tank is built up with discrete elements except for the series inductance which is integrated in the transformer. The secondary winding of the transformer has a midpoint connection and its turn ratio is 14:2:2. The values of the resonant tank elements are:

- Series inductance $L_s = 37\mu\text{H}$
- Series capacitance $C_s = 88\text{nF}$
- Parallel capacitance $C_p = 348\text{nF}$.

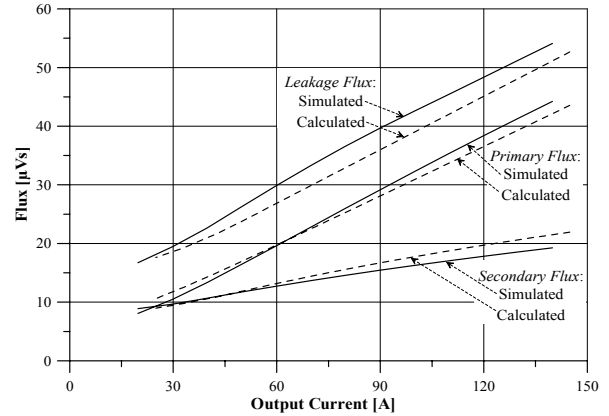


Fig. 7. Fluxes ($|\Phi_1|$, $|\Phi_2|$ and $|\Phi_1 + \Phi_2|$) in the three legs of the E-core against output current. *Solid lines:* results of simulations. *Broken lines:* predictions of proposed analytic model.

In **Fig. 9** the results for the operating frequency and for the duty cycle and in **Fig. 10/11** the results for the flux through the primary and the secondary winding and the leakage flux are given. There, the converter is just operating in the DCM due to the small value of the load resistance.



Fig. 8. Prototype of a 5kW/500kHz series-parallel resonant converter with ZCS in one and ZVS in the other leg.

The flux values can be measured by integrating the voltages across the windings. With this method the leakage flux is calculated as difference between the primary and the secondary flux. A more accurate method is to use a measurement winding (one turn) around the two legs of the core and the magnetic shunt and integrate the induced voltages. Therewith, the leakage flux could be measured directly.

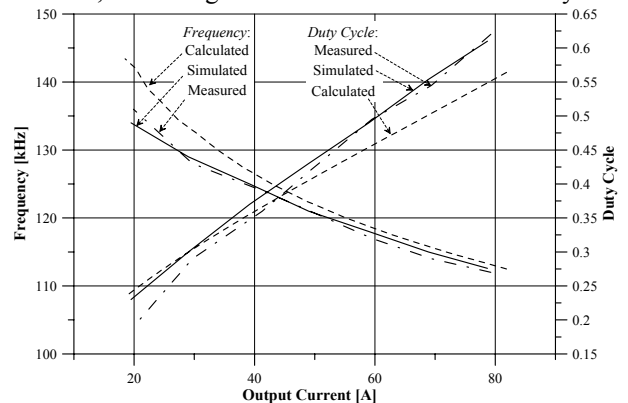


Fig. 9. Duty cycle D / frequency f against output current.
Solid lines: results of simulations.
Broken lines: predictions of proposed analytic model
Dot and dash line: measurement results.

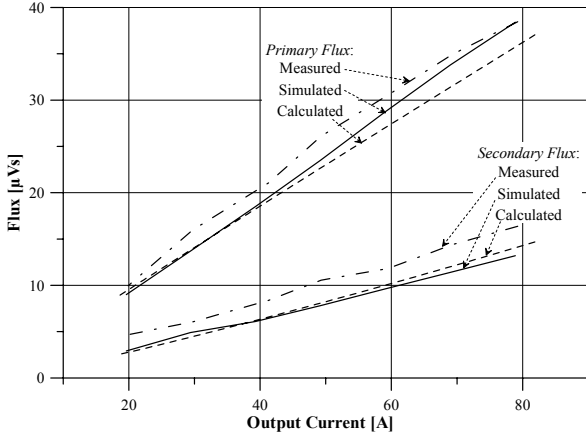


Fig. 10. Fluxes ($|\Phi_1|$ and $|\Phi_2|$) through the two windings against output current. *Solid lines*: results of simulations. *Broken lines*: predictions of proposed analytic model. *Dot and dash line*: measurement results.

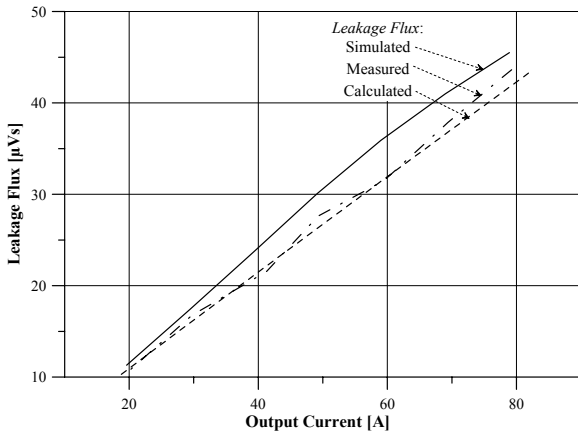


Fig. 11. Leakage Flux ($|\Phi_1 + \Phi_2|$) in the magnetic shunt of the E-core against output current. *Solid lines*: results of simulations. *Broken lines*: predictions of proposed analytic model. *Dot and dash line*: measurement results.

Again, the results for the analytic calculation, for the simulation and also for the measurement correspond very well.

Finally, the results for an electromagnetic integrated transformer shown in **Fig. 12** are presented. There, the series capacitance is realised by the primary winding and the parallel capacitance by the secondary winding. Moreover, the series inductance is implemented by increasing the leakage inductance of the transformer. The basic principles of integrating capacities and inductivities are explained in [7 - 10] and the design of the enclosing winding structure is presented in [10]. The values of the integrated resonant tank elements are:

- Series inductance $L_s = 21\mu\text{H}$
- Series capacitance $C_s = 37\text{nF}$
- Parallel capacitance $C_p = 115\text{nF}$.

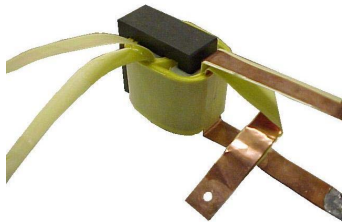


Fig. 12. Electromagnetically integrated transformer

With the electromagnetically integrated transformer the flux values in the different legs of the core must be measured with additional windings around the legs of the core (as described above). This is especially true for the primary winding since the measured voltage at the connections of the winding is the sum of the voltage across the series capacitance and the induced voltage which is not directly linked with the primary flux.

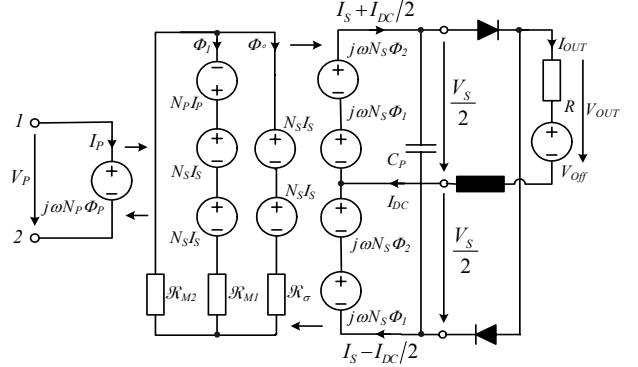


Fig. 13. Magnetic circuit diagram of the electromagnetically integrated transformer with rectifier and load

The reluctance model of the integrated transformer and the circuit diagram of the rectifier with load is given in **Fig 13**. The corresponding equations are given in (28).

$$\begin{aligned} N_p I_p &= \mathfrak{R}_{M1} \Phi_1 - \mathfrak{R}_\sigma \Phi_2 \\ 2N_s I_s &= -(\mathfrak{R}_\sigma \Phi_2 + \mathfrak{R}_{M2} \cdot (\Phi_1 + \Phi_2)) \end{aligned} \quad (28)$$

In **Fig. 14** the measured and calculated operating frequency and duty cycle against the output current are plotted and in **Fig. 15** the values for the primary, the secondary and the leakage flux are shown. Again, the converter is just operating in the DCM-mode due to the relation between the resonant tank elements and the load.

Remark: One leg of the converter is always switched at the zero crossing of the resonant current I_p (ZCS). In order to avoid for the complete load range that the anti-parallel diode of the MOSFET is turned off hardly the ZCS leg must be switched always a little bit before the zero crossing. This safety margin varies with the load current and also influences the actual switching frequency of the converter. This effect is not included in the proposed analytic model but could be included in the simulation.

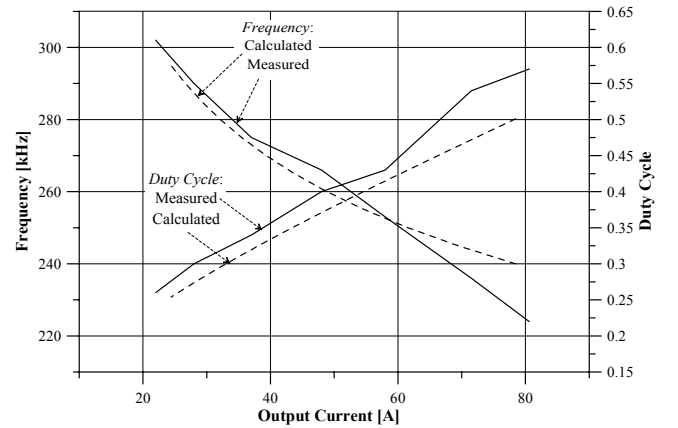


Fig. 14. Duty cycle D / frequency f against output current. *Solid lines*: measurement results. *Broken lines*: predictions of proposed analytic model

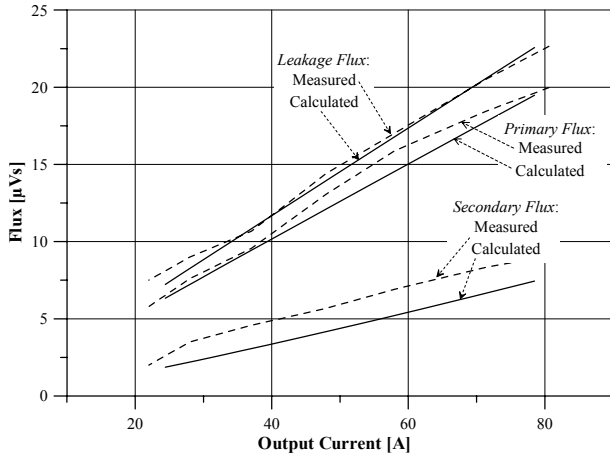


Fig. 15. Fluxes ($|\Phi_1|$, $|\Phi_2|$) and $|\Phi_1 + \Phi_2|$) in the different paths of the integrated core against output current. *Solid lines*: measurement results. *Broken lines*: proposed analytic model

The values predicted by the proposed calculation method are again in good correspondence with the measurement results.

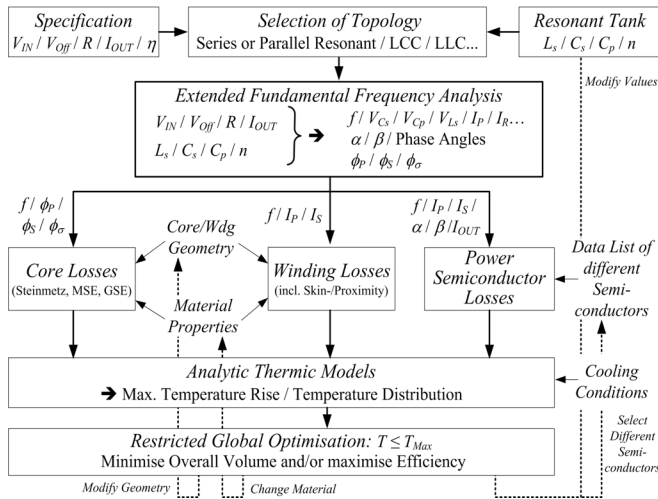


Fig. 16. Workflow of system optimisation procedure.

As shown above the proposed analytic model for the series-parallel resonant converter could be used to predict the operating frequency, the duty cycle, all the voltages and currents (amplitude and phase) and also the flux values in the core if the resonant tank elements, the input voltage, the load current and the load are given (cf. Fig. 16). With the predicted values the losses in the core, in the windings and also in the power semiconductors can be calculated. For this the geometry and material of the transformer and the technical data of the semiconductors is needed. Thereafter, the temperature rise and distribution of the magnetic device and the semiconductors could be calculated by an analytic thermal model. With the temperature rise and limit (T_{Max}) for the different components the converter now can be optimised for minimal overall volume or for maximum efficiency within a restricted volume. In order to achieve the optimum the transformer geometry, the applied materials, the power semiconductors and the values of the resonant tank elements are changed by the optimisation procedure.

With this procedure one just has to specify the input and output conditions of the converter and then the converter is optimally designed by the algorithm. The results of the optimisation for different applications are presented in future papers.

5. Conclusion

In this paper an analytic model for the series-resonant converter including the magnetic device is presented. This model includes also a ZCS condition for one leg of the converter and the control of the converter by frequency and duty cycle. The calculated results of the analytic model and for the flux distribution within the magnetic device correspond very well with the simulation and the measurement results presented for different resonant circuits.

With this model it is now possible to calculate the operating frequency, the duty cycle, all the current and voltage amplitudes and the flux distribution in the magnetic device for a given load and output current. With these results the losses in the transformer be calculated and the (integrated) magnetic device could be optimised (L_s , C_s and/or C_p integrated in the transformer). Moreover, the overall losses (including the core, the dielectric, the winding and also the semiconductor losses) can be predicted with the presented model and the whole system could be optimised in order to either minimise the losses or the overall volume.

References

- [1] G. A. Ward, A. J. Forsyth, "Topology selection and design trade-offs for multi-kW telecom DC power supplies", *International Conference on Power Electronics, Machines and Drives*, No. 487, June 4-7, 2002, pp. 439-444
- [2] F. Cavalcante, J. W. Kolar, "Design of a 5kW high output voltage series-parallel resonant DC-DC converter", *34th Power Electronics Specialist Conference*, Vol. 4, June 15-19, pp. 1807-1814
- [3] S. Dieckerhoff, M. J. Ruan, R. W. De Doncker, "Design of an IGBT-based LCL-resonant inverter for high-frequency induction heating", *Conference Record of 34th Industry Applications Conference*, Vol. 3, Oct. 3-7, 1999, pp. 2039-2045
- [4] A. K. S. Bhat, S. B. Dewan, "Analysis and design of a high-frequency resonant converter using LCC-type commutation", *IEEE Transaction on Power Electronics*, vol.2, No.4, 1987, pp. 291-300
- [5] R. L. Steigerwald, "A comparison of half-bridge resonant converter topologies", *IEEE Transactions on Power Electronics*, Vol. 3, Issue: 2, April, 1988 pp. 174-182
- [6] A. J. Forsyth, G. A. Ward, S. V. Mollov "Extended fundamental frequency analysis of the LCC resonant converter", *IEEE Transactions on Power Electronics*, Vol. 18, Issue 6, Nov., 2003, pp. 1286-1292
- [7] J. T. Strydom, "Electromagnetic design of integrated Resonator-Transformers", *Ph.D. Thesis, Rand Afrikaans University*, South Africa, 2001
- [8] M. C. Smit, J. A. Ferreira, J. D. van Wyk, "Application of transmission line principles to high frequency power converters", *23rd Power Electronics Specialists Conference*, Vol. 2, 29 June-3 July, 1992, pp. 1423-1430
- [9] I. W. Hofsaier, "On electromagnetic integration in hybrid electronic structures", *D. Eng. Thesis, Industrial and Electronics Research Group*, Faculty of Engineering, Rand Afrikaans University, May 1998
- [10] J. Biela, J. W. Kolar, "Electromagnetic integration of high power resonant circuits comprising high leakage inductance transformers", *35th Power Electronics Specialists Conference*, June 20-25, 2004, pp. 4537-4545
- [11] A. F. Witulski, "Introduction to modelling of transformers and coupled inductors", *IEEE Transactions on Power Electronics*, Vol. 10, Issue 3, May, 1994, pp. 349-357
- [12] A. Balakrishnan, W. T. Joines, T. G. Wilson, "Air-Gap reluctance and inductance calculations for magnetic circuits using Schwarz-Christoffel Transformation", *IEEE Transactions on Power Electronics*, Vol. 12, Issue 4, 1997, pp. 654-663
- [13] R. C. Roters, "Electromagnetic Devices", John Wiley & Sons, 1941
- [14] A. F. Hoke, C. R. Sullivan, "An improved two-dimensional numerical modelling method for E-Core Transformers", *17th Applied Power Electronics Conference and Exposition*, Vol. 1, March 10-14, 2002, pp. 151-157
- [15] C. P. Steinmetz, "On the law of hysteresis", *Proc. IEEE*, vol. 72, February 1984, pp. 196-221